

# Detection and Visualization of Macro Defects in Color Liquid Crystal Displays through Gabor Transforms

Hiroki Nakano <sup>†</sup>  
IBM Japan, Ltd.

Yasuo Yoshida <sup>††</sup>  
Faculty of Engineering and  
Design, Kyoto Institute of  
Technology

## Abstract

This paper proposes a novel approach for detecting macro defects in color LCDs (liquid crystal displays) by using 2-D Gabor coefficients. The absolute value of the complex Gabor coefficients of an input image are used to detect macro defects such as periodic or streak patterns. The paper also proposes a new method for reconstructing images with reduced noise through linear combination of 2-D Gabor coefficients. The reconstructed images can help human evaluators to verify defects. The number of reconstruction coefficients to be decided is only 1/256 of that in Daugman's method using a linear combination of the Gabor functions. This greatly reduces computational complexity of the proposed method. Experiments on actual defect images showed the effectiveness of the method.

## 1 Introduction

A color LCD (liquid crystal display) is one of main components of a mobile personal computer. A color filter plays a key role of adding color to the display (Fig. 1). It is placed above the liquid crystal layer, and consists of red, green, and blue cells arranged in order. Macro defects such as periodic or streak patterns on the color filter cause unevenness in the luminescence of the display. It is very difficult for human evaluators to detect macro defects on the color filter, because the contrast between the macro defects and the background is too weak to observe.

This paper has two main objectives.

The first is to detect macro defects with unknown modulation frequencies and orientations. For this purpose, the paper proposes using the absolute value of Gabor coefficients as feature measures. The Gabor coefficients are generated by convolution of the Gabor functions and the observed image, and these self-similar Gabor functions are configured in the frequency domain. The reason for using the Gabor functions is that it is effective for defect

detection to calculate the correlation between Gabor functions and macro defects [1]-[4].

The second objective is to display defect-enhanced images. This paper proposes a new method for reconstructing defect-enhanced images by using a linear combination of real parts of Gabor coefficients. The uniqueness of this method is that not all coefficients are used, but only those that contribute to defect detection. The number of reconstruction coefficients to be decided is only 1/256 of that in Daugman's method using a linear combination of Gabor functions [5].

## 2 Gabor functions

The 2-D Gabor function used in this paper is defined as:

$$G_j(x, y) = \kappa e^{-\frac{1}{4\pi\sigma_j^2}(x^2+y^2)} e^{ju_i x},$$

$$\begin{bmatrix} \dot{x} \\ \dot{y} \end{bmatrix} = \begin{bmatrix} \cos\phi_i & \sin\phi_i \\ -\sin\phi_i & \cos\phi_i \end{bmatrix} \begin{bmatrix} x \\ y \end{bmatrix}, \quad (1)$$

where

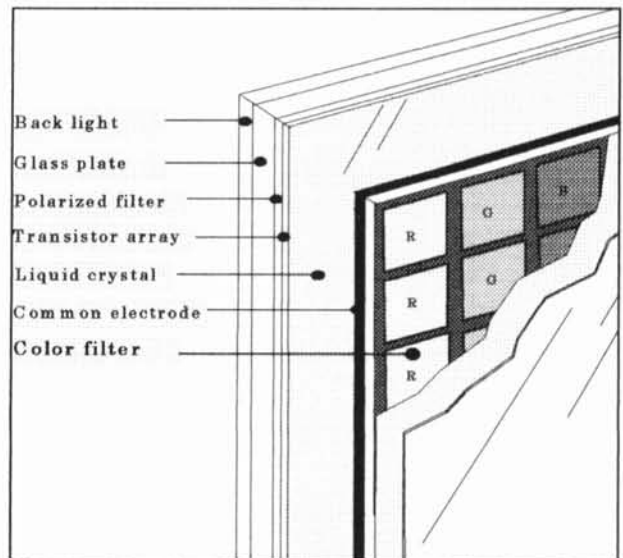


Fig. 1. Structure of a color active matrix liquid crystal display

<sup>†</sup> Address: 800 Yasu Shiga 520-23, Japan.

E-mail: hnakano@vnet.ibm.com

<sup>††</sup> Address: Kyoto 606, Japan.

E-mail: yyoshida@dj.kit.ac.jp

$$\kappa = \frac{1}{4\pi^2 \sigma_i^2} \quad (2)$$

$\dot{x}$  and  $\dot{y}$  are axes that are rotated by  $\phi_i$ , while  $u_i$  and  $\sigma_i$  are the modulation frequency and the scale parameter of the Gaussian window.  $\kappa$  is a factor for normalizing maximum value of  $G_i(x, y)$  in frequency domain. The Gabor coefficient  $a_i(x, y)$  is given by convolution of the input image  $s(x, y)$  and the Gabor function with parameter set  $(\sigma_i, u_i, \phi_i)$ :

$$a_i(x, y) = \int_{-\infty}^{\infty} \int_{-\infty}^{\infty} s(x', y') G_i(x-x', y-y') dx' dy' \quad (3)$$

The Fourier transform of (1) is given by the formula

$$\hat{G}_i(u, v) = e^{-\pi\sigma_i^2[(u-u_i)^2+v^2]},$$

$$\begin{bmatrix} \dot{u} \\ \dot{v} \end{bmatrix} = \begin{bmatrix} \cos\phi_i & \sin\phi_i \\ -\sin\phi_i & \cos\phi_i \end{bmatrix} \begin{bmatrix} u \\ v \end{bmatrix} \quad (4)$$

### 3 Detecting macro defects by using Gabor functions

This section proposes using the absolute value of Gabor coefficients as feature measures for detecting macro defects with spatial frequencies and orientations such as streak or periodic patterns. In a 2-D coefficient image, if there are many enough pixels which values exceed a predetermined threshold, we determine that some defects exist in the frequency range of the Gabor filter  $G_i(x, y)$ .

#### 3.1 Gabor coefficients

To keep constant the effective wave number in the Gaussian window regardless of the modulation frequency of the Gabor function, we add the following condition to (1):

$$u_i \sigma_i = k \quad (5)$$

(constant  $k$  is invariant with  $i$ ).

This idea is based on the wavelet scheme such that the product of the modulation frequency  $u_i$  and the position accuracy  $\sigma_i$  is constant [6]-[8]. To utilize the Gabor function as a band-pass filter for detection of macro defects, the DC component of the Gabor function should be zero. The DC component of the Gabor function is derived from (4):

$$\hat{G}_i(0,0) = e^{-\pi k^2} \quad (6)$$

Therefore,  $\hat{G}_i(0,0)$  is approximately zero when  $k$  is large enough.

By means of an example, we show that the absolute value of coefficients reflect the intensity of the defects. In this example, we assume that the periodicity of macro defects is kept within the Gaussian window with scale parameter  $\sigma_i$ . The original image  $s(x, y)$  is defined as follows:

$$s(x, y) = b_0 + b_1 \cos(\omega\dot{x} + \theta),$$

$$\dot{x} = x \cos\psi + y \sin\psi \quad (7)$$

If (6) is approximately zero, the Gabor coefficient of (7) is

$$a_i(x, y) = \iint s(x', y') G_i(x-x', y-y') dx' dy'$$

$$\cong \frac{1}{2} b_1 e^{j(\omega\dot{x} + \theta)} e^{-\pi\sigma_i^2 d_i^2} \quad (8)$$

where

$$\dot{x} = x \cos\psi + y \sin\psi \quad (9)$$

$$d_i^2 = (u_i \cos\phi_i - \omega \cos\psi)^2 + (u_i \sin\phi_i - \omega \sin\psi)^2 \quad (10)$$

$d_i$  denotes the distance between  $(u_i, \phi_i)$  and  $(\omega, \psi)$  in the frequency domain. The absolute value of coefficient  $|a_i(x, y)|$  is

$$|a_i(x, y)| \cong \frac{1}{2} b_1 e^{-\pi\sigma_i^2 d_i^2} \quad (11)$$

Thus, assuming that  $(\omega, \psi)$  is nearly equal to one of the modulation parameter  $(u_i, \phi_i)$ , periodic defects with a set of parameters  $(\omega, \psi)$  can be detected, because (11) becomes approximately  $b_1/2$ .

#### 3.2 Noise improvement rate

To measure the filter performance, we now define the improvement rate of the signal-to-noise ratio (*IRSNR*). This is an index of the filter performance for defect detection when the observed image contains noise. We then redefine an original image with noise  $W(x, y)$  as follows:

$$s(x, y) = b_0 + b_1 \cos(\omega\dot{x} + \theta) + W(x, y),$$

$$\dot{x} = x \cos\psi + y \sin\psi \quad (12)$$

where  $W(x, y)$  is white noise and has the following natures:

$$E[W(x, y)] = 0 \quad (13)$$

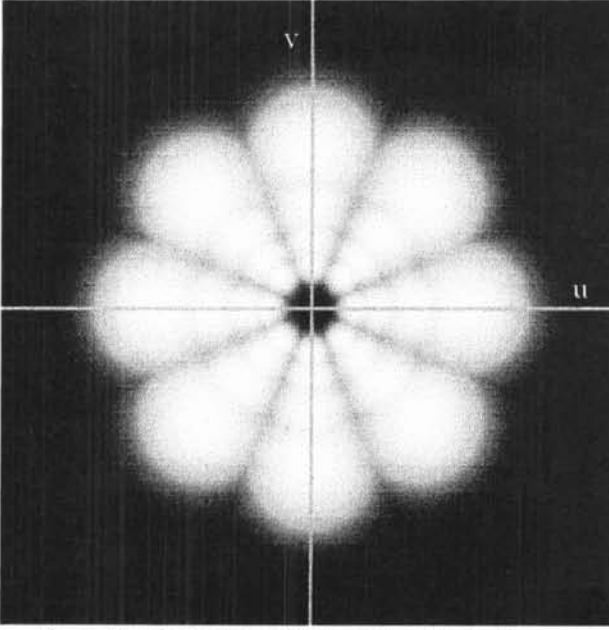


Fig. 2. Configuration of Gabor filters in the frequency domain

$$E[W(x,y)W(x',y')] = \sigma_w^2 \delta(x-x')\delta(y-y'), \quad (14)$$

where  $E[\cdot]$  is the expected value,  $\delta(\cdot)$  is the delta function, and  $\sigma_w^2$  denotes the variance of  $W(x,y)$ .

We then obtain the Gabor coefficient

$$\begin{aligned} a_i(x,y) &= \iint s(x',y')G_i(x-x',y-y')dx'dy' \\ &\cong \frac{1}{2} b e^{j(\omega\dot{x}+\theta)} e^{-\pi\sigma_i^2 d_i^2} + U(x,y), \end{aligned} \quad (15)$$

where  $\dot{x}$  and  $d_i$  are defined by (9) and (10), and

$$U(x,y) = \iint W(x',y')G_i(x-x',y-y')dx'dy'. \quad (16)$$

In this paper, the signal-to-noise ratio (SNR) is defined as the ratio of the square of the intensity of the signal to the variance of noise [10]. Thus we can obtain the SNR of the original image and the SNR of the coefficient image as

$$SNR_{IN} = \frac{b_1^2}{\sigma_w^2} \quad (17)$$

$$\begin{aligned} SNR_{OUT} &= \frac{b_1^2 e^{-2\pi\sigma_i^2 d_i^2}}{4E[|U(x,y)|^2]} \\ &= \frac{2\pi^2 \sigma_i^2 b_1^2 e^{-2\pi\sigma_i^2 d_i^2}}{\sigma_w^2} \end{aligned} \quad (18)$$

(see the appendix for the derivation of the equation).

Now the  $IRSNR$  is defined as the ratio of  $SNR_{OUT}$  to  $SNR_{IN}$ :

$$\begin{aligned} IRSNR &= \frac{SNR_{OUT}}{SNR_{IN}} \\ &= 10\log_{10}(2\pi^2 \sigma_i^2 e^{-2\pi\sigma_i^2 d_i^2}) \quad [\text{dB}]. \end{aligned} \quad (19)$$

### 3.3 Configuration of Gabor filters in the frequency domain

We now consider the configuration of Gabor filters in the frequency domain. The frequency domain in which defects exist is bounded, and known empirically. To detect any types of defect with unknown modulation frequencies and orientations, Gabor filters are placed densely within the frequency domain. Therefore we set rotationally symmetric Gabor filters  $\hat{G}_i(u,v)$  in the bounded frequency domain [5],[9]. These filters are configured in the manner that the  $IRSNR$  shown in (19) is higher than a threshold everywhere in the frequency domain. An example of the filter configuration is shown in Fig. 2.

### 4 Reconstruction of the image from Gabor coefficients

Jain reported that an original image can be reconstructed by a linear combination of the real parts of Gabor coefficients [11]. Therefore, we assume that  $s(x,y)$  is approximately represented by  $\tilde{s}(x,y)$ :

$$\tilde{s}(x,y) = \sum_i c_i a_i^{\text{Re}}(x,y). \quad (20)$$

Taking the example given by (7), we obtain

$$\tilde{s}(x,y) \cong \frac{1}{2} b_1 \cos(\omega\dot{x} + \theta) \sum_i c_i e^{-\pi\sigma_i^2 d_i^2}, \quad (21)$$

where  $\dot{x}$  and  $d_i$  are defined by (9) and (10).

Thus, if  $\sum_i c_i e^{-\pi\sigma_i^2 d_i^2}$  is regarded as a constant independent of  $(\omega, \psi)$  in (7), we can conclude that  $\tilde{s}(x,y)$  represents the intensity and wave form of the original image ((7)).

The purpose in this section is to display a defect-enhanced image in order to show the result of detection. Then, to reconstruct the noise-reduced image, we should not use all the coefficients, but only the coefficients  $a_i^{\text{Re}}(x,y)$  related to the modulation frequencies and orientations of the macro defects. According to Jain's paper, all reconstruction coefficients in (20) are constant ( $c_i = 1$ ). To obtain more precise coefficients, the least square method can be used. We define the distance

between  $s^*(x, y)$  and  $\tilde{s}(x, y)$  as follows:

$$D = \|s^*(x, y) - \tilde{s}(x, y)\|^2 = \iint |s^*(x, y) - \tilde{s}(x, y)|^2 dx dy, \quad (22)$$

where

$$s^*(x, y) = \frac{1}{2\pi} \iint \hat{s}(u, v) \hat{h}(u, v) e^{j(u x + v y)} du dv \quad (23)$$

and  $\hat{s}(u, v)$  denotes the Fourier transform of  $s(x, y)$ .

$\hat{h}(u, v)$  is a function shown by the following formula in the frequency domain (see Fig. 2):

$$\hat{h}(u, v) = \begin{cases} 1 & \text{(inside Gabor filters used for reconstruction)} \\ 0 & \text{(elsewhere)} \end{cases}. \quad (24)$$

$\hat{h}(u, v)$  is 1 in the region where the absolute values of the Gabor filters used for reconstruction are larger than those of other Gabor filters in frequency domain.

Thus,  $s^*(x, y)$  indicates the inverse Fourier transform of  $\hat{s}(u, v)$  with the frequency domain limited by  $\hat{h}(u, v)$ .

We can obtain the following formula by using Parseval's identity

$$D = \frac{1}{4\pi^2} \iint |\hat{s}^*(u, v) - \sum_i c_i \hat{a}_i^{\text{Re}}(u, v)|^2 du dv, \quad (25)$$

where

$$\hat{a}_i^{\text{Re}}(u, v) = \mathcal{F}[a_i^{\text{Re}}(x, y)] \quad (26)$$

( $\mathcal{F}[\cdot]$  denotes the Fourier transform),

and where

$$\hat{a}_i^{\text{Re}}(u, v) = \hat{s}(u, v) \hat{G}_i^{\text{Re}}(u, v) \quad (27)$$

$$\hat{s}^*(u, v) = \hat{s}(u, v) \hat{h}(u, v) \quad (28)$$

$$\hat{G}_i^{\text{Re}}(u, v) = \mathcal{F}[\text{Re}(G_i(x, y))]. \quad (29)$$

By rewriting (25), we obtain

$$D = \frac{1}{4\pi^2} \iint |\hat{s}(u, v)|^2 \times (\hat{h}(u, v) - \sum_i c_i \hat{G}_i^{\text{Re}}(u, v))^2 du dv. \quad (30)$$

To minimize  $D$ , all  $c_i$  must satisfy the following equation:

$$\begin{aligned} \frac{\partial D}{\partial c_i} &= \frac{-1}{2\pi^2} \iint \{|\hat{s}(u, v)|^2 \hat{G}_i^{\text{Re}}(u, v) \\ &\quad \times (\hat{h}(u, v) - \sum_j c_j \hat{G}_j^{\text{Re}}(u, v))\} du dv \\ &= 0. \end{aligned} \quad (31)$$

By rewriting this equation, we obtain

$$\mathbf{A}\mathbf{C}^T = \mathbf{B}^T \quad (32)$$

The components of the matrix  $\mathbf{A}$  and the vector  $\mathbf{B}$  are

$$\mathbf{A}_{i,j} = \iint \{|\hat{s}(u, v)|^2 \hat{G}_i^{\text{Re}}(u, v) \hat{G}_j^{\text{Re}}(u, v)\} du dv \quad (33)$$

$$\mathbf{B}_i = \iint |\hat{s}(u, v)|^2 \hat{h}(u, v) \hat{G}_i^{\text{Re}}(u, v) du dv \quad (34)$$

The components of the vector  $\mathbf{C}$  are  $c_i$ , which can be obtained by calculating the inverse matrix of  $\mathbf{A}$ .

## 5 Experimental results

An experiment of defect detection was performed for a color filter that had defects with unknown modulation frequencies and orientations. The size of the original image was  $256 \times 256$  pixels with 256 gray levels. Figs. 3(a) and 3(c) show the original image and the reconstructed image, respectively. Fig. 3(b) represents the absolute value of the Gabor coefficients for 16 different parameter sets. For the original image, we chose a color filter containing macro defects consisting of streak patterns with several orientations. The number of combinations of  $u_i$  and  $\phi_i$  of Gabor functions was  $16 : u_i = \{0.1, 0.15, 0.23, 0.34\}$ ,  $\phi_i = \{0^\circ, 45^\circ, 90^\circ, 135^\circ\}$ , where  $\sigma_i = k / u_i$  and  $k = 1.2$  for all  $i$ . In this case, the difference between the maximum and minimum of the IRSNR shown by (19) was 6[dB] at most. The maximum of the IRSNR appears when the modulation frequency and orientation of a defect are equal to those of one of the Gabor filters. On the other hand, the minimum appears in the valley between the Gabor filters in the frequency subdomain (Fig. 2).

In Fig. 3(b), three images with the parameter sets  $\{u_i = 0.1, \phi_i = 45^\circ\}$ ,  $\{u_i = 0.15, \phi_i = 45^\circ\}$ , and  $\{u_i = 0.23, \phi_i = 135^\circ\}$  contain bright and large white regions. In these images, the number of pixels exceeding a predetermined value exceeded a threshold. We thus determined that macro defects could be observed in the three images.

The defect-enhanced image was then reconstructed by a linear combination of the real parts of these three images (Fig. 3(c)). The reconstruction coefficients were calculated by solving (32). As a result, streak patterns with

orientations of  $45^\circ$  and  $135^\circ$  can be easily recognized in Fig. 3(c).

## 6 Comparison with Daugman's method

The image reconstruction method proposed in this paper consists of a linear combination of the real parts of coefficients. On the other hand, the method proposed by Daugman, which is a well-known for image reconstruction [5], consists of the linear combination of Gabor functions. In the Daugman's method, the maximum number of reconstruction coefficients to be decided would be 4096, if this method were used for visualization of macro defects. By using the method proposed in this paper, the maximum number of reconstruction coefficients to be decided is only 16. This gives the proposed method a great advantage in terms of computational complexity.

## 7 Conclusion

This paper has proposed a method using Gabor coefficients for detecting macro defects in color LCDs and for visualizing recognition results. The absolute value of the complex Gabor coefficients of an input image are used to detect macro defects such as periodic or streak patterns. The paper also proposed a new method for reconstructing images with reduced noise through linear combination of the 2-D Gabor coefficients. The reconstructed images can help human evaluators to verify defects. The number of reconstruction coefficients to be decided is only 1/256 of that in Daugman's method using a linear combination of Gabor functions. Experimental results using actual defect images showed the effectiveness of the method. This method is practical in terms of its computational complexity, and can thus be used for on-line automatic inspection.

## Appendix

### Proof of (18)

We have

$$\begin{aligned}
 E[|U(x, y)|^2] &= \\
 & \iint \iint G_i(x - x', y - y') G_i(x - x'', y - y'') \\
 & \quad \times E[W(x', y') W(x'', y'')] dx' dy' dx'' dy'' \\
 &= \sigma_w^2 \iint |G_i(x - x', y - y')|^2 dx' dy' \\
 &= \frac{\sigma_w^2}{4\pi^2} \iint |\hat{G}_i(u, v)|^2 dudv. \quad (A.1)
 \end{aligned}$$

Thus

$$E[|U(x, y)|^2] = \frac{\sigma_w^2}{8\pi^2 \sigma_i^2}. \quad (A.2)$$

## References

- [1] D. Casasent, J. S. Smokelin, and A. Ye: "Optical Gabor and wavelet transform for scene analysis," Proc. SPIE Hybrid Image & Signal Process. III, Vol. 1702, pp. 2-10, Apr. 1992.
- [2] R. N. Braithwaite and B. Bhanu: "Hierarchical Gabor filter for object detection in infrared images," Proc. IEEE Comput. Vision & Pattern Recog. '94, pp. 628-631, Jun. 1994.
- [3] M. H. Gross and R. Koch: "Visualization of multidimensional shape and texture features in laser range data using complex valued Gabor wavelets," IEEE Trans. Vis. & Comput. Graphics, Vol. 1, No. 1, pp. 44-59, Mar. 1995.
- [4] J. Ben Arie and K. R. Rao: "Novel approach to template recognition by image expansion with non-orthogonal wavelets," Proc. SPIE Visual Communications and Image Processing '92, Vol. 1818, pp. 991-1003, Nov. 1992.
- [5] J. G. Daugman: "Complete discrete 2-D Gabor transform by neural networks for image analysis and compression," IEEE Trans. Acoust., Speech & Signal Process., Vol. 36, pp. 1169-1179, July 1988.
- [6] A. C. Bovik, M. Clark, and W.S. Geisler: "Multichannel texture analysis using localized spatial filters," IEEE Trans. Pattern Anal. & Mach. Intell., Vol. 12, No. 1, pp. 55-73, Jan. 1990.
- [7] K. Kawata and S. Arimoto: "Hierarchical texture analysis using Gabor expansion," Trans. IEICE D-II, Vol. J78, pp. 437-444, Mar. 1995.
- [8] C. K. Chui: "An introduction to wavelets," Academic press, 1992.
- [9] S. Mallat: "Wavelets for a vision," Proc. IEEE, Vol. 84, No. 4, pp. 604-614, Apr. 1996.
- [10] B. V. K. Vijara Kumar and L. Hassebrook: "Performance measurements for correlation filters," Appl. Opt., Vol. 29, No. 20, pp. 2997-3006, July 1990.
- [11] A. K. Jain and F. Farrokhnia: "Unsupervised texture segmentation using Gabor filters," Pattern Recognition, Vol. 24, No. 12, pp. 1167-1186, 1991.



Fig. 3(a) Original image



Fig. 3(c) Defect enhanced image

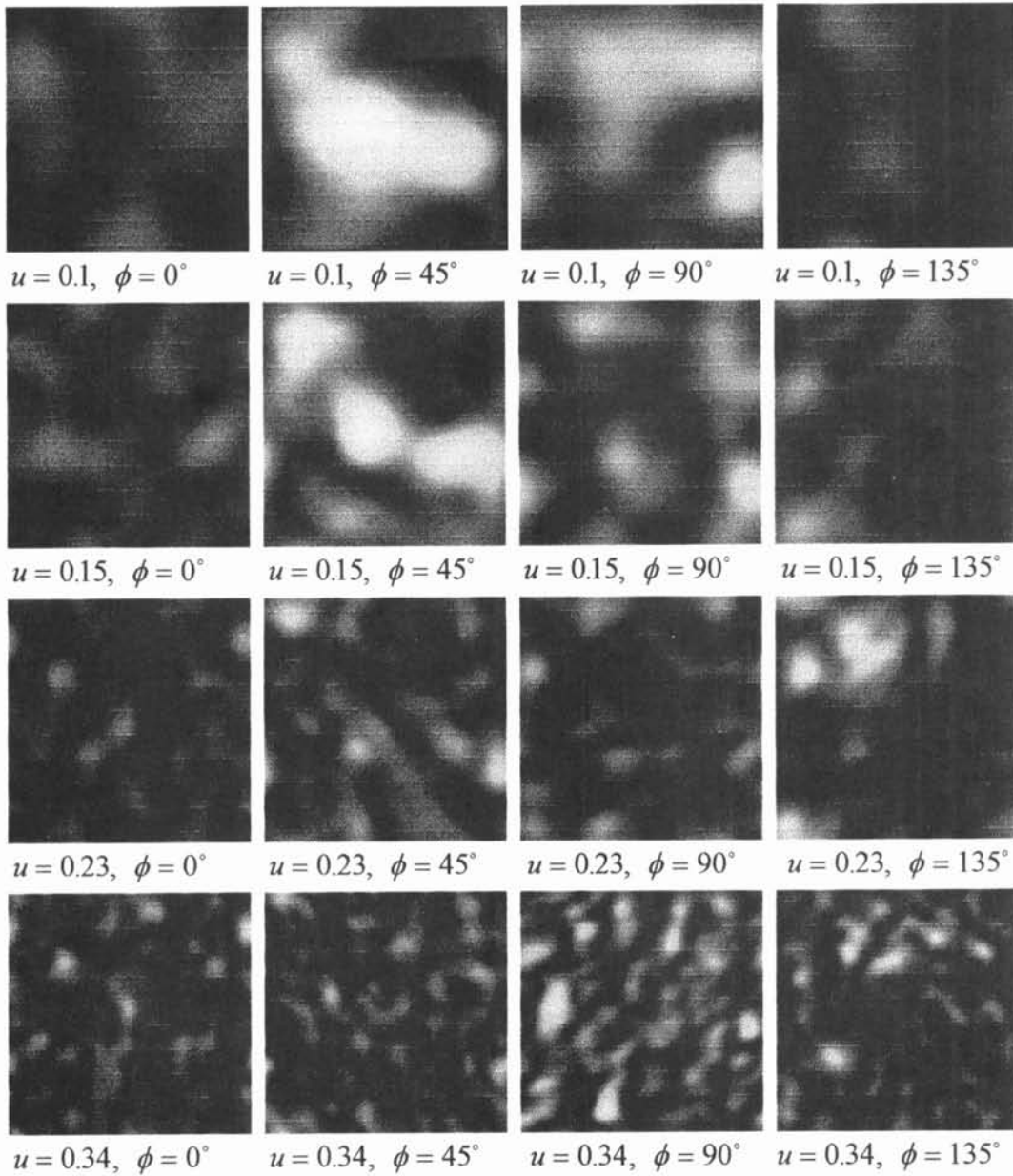


Fig. 3(b) Coefficient images (absolute value)